# Transport through cavities with tunnel barriers: a semiclassical analysis

M. Schreier[1], K. Richter[2], G.-L. Ingold[1,a], and R.A. Jalabert[3]

[1] Institut für Physik, Universität Augsburg, 86135 Augsburg, Germany
[2] Max-Planck-Institut für Physik komplexer Systeme, Nöthnitzer Str. 38, 01187 Dresden, Germany
[3] Université Louis Pasteur, IPCMS-GEMME, 23 rue du Loess, 67037 Strasbourg Cedex, France

**Abstract.** We study the influence of a tunnel barrier on the quantum transport through a circular cavity. Our analysis in terms of classical trajectories shows that the semiclassical approaches developed for ballistic transport can be adapted to deal with the case where tunneling is present. Peaks in the Fourier transform of the energy-dependent transmission and reflection spectra exhibit a nonmonotonic behaviour as a function of the barrier height in the quantum mechanical numerical calculations. Semiclassical analysis provides a simple qualitative explanation of this behaviour, as well as a quantitative agreement with the exact calculations. The experimental relevance of the classical trajectories in mesoscopic and microwave systems is discussed.

**PACS.** 73.23.Ad Ballistic transport – 03.65.Sq Semiclassical theories and applications

## 1 Introduction

Ballistic transport through quantum billiards has been extensively studied in recent years due to its relevance for quantum chaos and the possibility of physical applications. Realizations of ballistic billiards include structured two-dimensional electron gases in semiconductor heterostructures [1,2] and, exploiting the analogy between quantum and wave mechanics, microwave cavities [3]. Various experiments have been designed to test theoretical ideas on conductance fluctuations [4–6], weak localization [7–10] and the signatures of classical integrability. The main theoretical tool for making the connection between the quantum and classical properties is the semiclassical expansion [11,12]. This intuitive and powerful approach has been tested numerically for the transport through circular cavities [13–15]. In particular, the identification of the most relevant trajectories for transmission and reflection has been accurately demonstrated (analogously to the relationship between the density of states and periodic orbits of closed systems [11]). Moreover, the semiclassical approach has been extended by the inclusion of diffraction effects at the entrance and exit of the cavities [15].

In this work we further extend the applicability of semiclassical methods in open systems to treat the case where tunneling takes place. The modification of the trace formula in a closed system by the inclusion of a potential step has recently been addressed for a circular billiard [16] in the context of ray splitting. There the possibility of electrons entering in the region of higher potential has to be taken into account. Our work shows that a tunnel barrier within a cavity can very simply be incorporated in a semiclassical description and changes the relative importance of different classical trajectories in a non-trivial manner. Our interest in tunneling inside a cavity stems from a fundamental point of view as well as from the fact that experiments with a high potential barrier within a quantum dot (pacman) have already been performed [17]. In microwave billiards tunnel barriers could be realized if the cavity were filled with a dielectric except for a thin slit which acts as a barrier.

Starting from the well-studied circular billiard [13–15], we introduce a thin barrier placed symmetrically between the two leads and extending from the edge to the center of the circle as shown by the dashed line in Figure 1. The barrier height $V_b$ is variable and allows to interpolate between a circle and the billiard studied in reference [17]. Of special interest will be the regime where the electron energy is of the order of the barrier height so that tunneling becomes relevant. In the following, we therefore refer to this billiard as the circular tunneling billiard.

We will consider phase coherent and ballistic transport through the cavity which is attached to two hard-wall leads of width $W$. For a fixed energy $E$ of the incident particles there exists only a finite number of transverse modes $N$, given by the largest integer smaller than $(E/E_0)^{1/2}$, which contribute to the transport. Here,

$$E_0 = \frac{\hbar^2\pi^2}{2MW^2} \tag{1}$$

[a] e-mail: Gert.Ingold@Physik.Uni-Augsburg.de

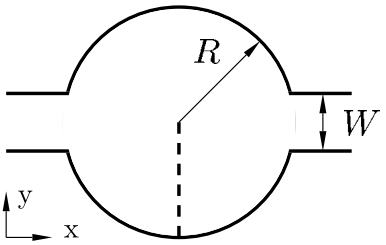


**Fig. 1.** The circular tunneling billiard consists of a circular billiard of radius $R$ attached to two opposite leads of width $W$ and a thin potential barrier of variable height shown as dashed line reaching from the edge to the center of the circle.

is the energy of the lowest transverse mode in the leads and $M$ is the mass of the particles.

Within the Landauer formalism [1,2] the two-probe conductance $g$ through the structure is just proportional to the total transmission coefficient $T$ at the Fermi energy $E_F$

$$g = \frac{e^2}{h}\, T = \frac{e^2}{h}\, \sum_{n,m} |t_{nm}|^2. \tag{2}$$

The transmission amplitude connecting the incoming mode $m$ to the outgoing mode $n$ is given by the projection [18,19]

$$G_{nm}(x', x, E_F) = \int_0^W \int_0^W \mathrm{d}y' \mathrm{d}y\, G(x', y', x, y, E_F) \chi_n(y') \chi_m(y) \tag{3}$$

of the retarded Green function $G(x', y', x, y, E_F)$ of the structure onto the transverse modes

$$\chi_m(y) = \sqrt{\frac{2}{W}} \sin\Big(\frac{\pi m}{W} y\Big) \tag{4}$$

according to

$$t_{nm} = \frac{\mathrm{i}\hbar^2}{M} (k_m k_n)^{1/2} G_{nm}(x', x, E_F), \tag{5}$$

where we have discarded an unimportant phase factor. The longitudinal wave vector is given by

$$k_n = \left( \frac{2M(E - n^2 E_0)}{\hbar^2} \right)^{1/2}. \tag{6}$$

The expression (3) has to be evaluated with $x$ in the incoming and $x'$ in the outgoing lead. For the amplitude of reflection one finds the corresponding expression

$$r_{nm} = -\delta_{nm} + \frac{\mathrm{i}\hbar^2}{M} (k_m k_n)^{1/2} G_{nm}(x', x, E_F). \tag{7}$$

with $x$ and $x'$ in the incoming lead.

The transmission and reflection amplitudes can be obtained numerically by means of the recursive Green function method [20,21]. This method uses a discretized version of the cavity and calculates the Green function by starting from the exact Green function in one of the leads and successively building up the solution by means of the Dyson equation.

Alternatively, a semiclassical approach to transport can be developed from the semiclassical path-integral form of the Green function leading to a transmission amplitude [12]

$$t_{nm} = -\frac{\sqrt{2\pi\mathrm{i}\hbar}}{2W} \sum_{s(\bar{n},\bar{m})} \mathrm{sgn}(\bar{n})\mathrm{sgn}(\bar{m}) \sqrt{\tilde{D}_s} \times \exp\left( \frac{\mathrm{i}}{\hbar} \tilde{S}_s(\bar{n}, \bar{m}, E_F) - \mathrm{i}\frac{\pi}{2} \tilde{\mu}_s \right), \tag{8}$$

given as the sum over classical trajectories $s$ between the entrance and exit cross sections with incoming and outgoing angles $\theta$ and $\theta'$ such that $\sin\theta = \bar{m}\pi/kW$ and $\sin\theta' = \bar{n}\pi/kW$ ($\bar{m} = \pm\, m$, $\bar{n} = \pm\, n$). The reduced action $\tilde{S}$ is the Legendre transform of the action integral $S$,

$$\tilde{S}(\bar{n}, \bar{m}, E_F) = S(y_0', y_0, E_F) + \frac{\hbar\pi}{W}(\bar{m} y_0 - \bar{n} y_0'), \tag{9}$$

where the starting and end points of the trajectory, $y_0$ and $y_0'$ respectively, are determined by the angle quantization. For billiards $S/\hbar = kL$, where $L$ is the length of the trajectory. The amplitude is $\tilde{D} = (Mv|\cos\theta'|)^{-1} |(\partial y/\partial\theta')_\theta|$ and $\tilde{\mu}$ is the Maslov index. A similar expression holds for the reflection amplitude, with the difference that now the trajectories start and end in the same lead.

Direct comparison between the semiclassical amplitudes (or the conductance) and the exact counterparts is rather difficult since the expansion (8) includes an infinite number of terms associated with an exponentially large number of contributing classical trajectories. However, as in the case of the trace formula, the validity of the semiclassical approach can be established by identifying the Fourier components of $t_{nm}$ with classical trajectories. This has been done in reference [15] and we verify it in our system since it gives the starting point of our analysis.

In Section 2 we present the numerical calculation of the reflection amplitude and its interpretation in terms of classical trajectories without and with a high barrier. In Section 3 we consider the influence of a tunnel barrier on the different trajectories contributing to the reflection and transmission amplitudes and find a nonmonotonic behaviour. This behaviour is modeled in Section 4 within a modification of the semiclassical transmission amplitudes that includes tunneling in a very simple way. In Section 5 we consider a similar analysis for the transmission and reflection coefficients, and show that the analysis becomes considerably more involved since we now have to deal with pairs of trajectories. In the final section we present our conclusions and discuss the extension of our work to the case with magnetic field.

## 2 Identification of classical trajectories

In Figure 2 we present the (exact) total reflection coefficient together with the contribution from the lowest mode

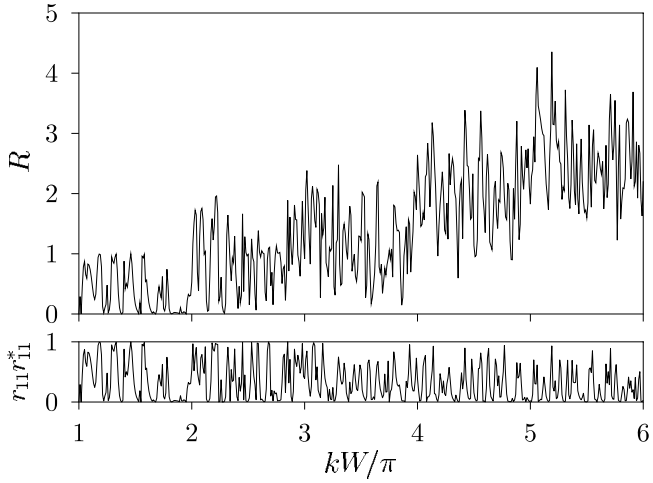


**Fig. 2.** Total reflection of the circular billiard and the squared modulus of $r_{11}$ as a function of the Fermi momentum. For $1 < kW/\pi < 2$, both reflection coefficients coincide as there is only one propagating mode.

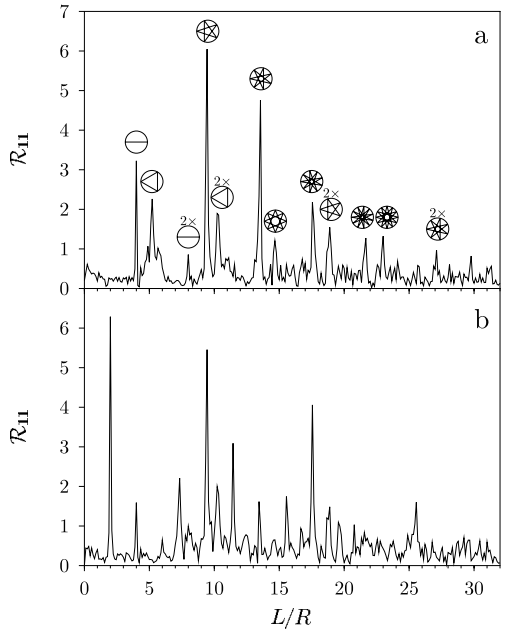


**Fig. 3.** Length spectrum $\mathcal{R}_{11}$ for (a) the case without a barrier and (b) with an infinitely high barrier. Lengths are scaled to the radius $R$ of the circle. In the absence of a barrier we identify the peaks in the length spectrum with periodic trajectories.

$|r_{11}|^2$. Obviously, for $1 < kW/\pi < 2$ the two quantities coincide since there $N = 1$. In order to identify the classical trajectories we carried out a discrete Fourier transformation of 600 values of the complex reflection amplitude $r_{11}$ calculated over a momentum interval ranging from 1 to $7\pi/W$. The ratio between the radius $R$ of the circle and the width $W$ of the leads was in all calculations taken to be $R/W = 3$.

The semiclassical form (8) of the transmission amplitude implies that its Fourier transform with respect to the momentum $k = (2ME_F/\hbar^2)^{1/2}$ should exhibit peaks at lengths $L$ corresponding to the contributing classical trajectories. Similarly, the reflection amplitudes can be interpreted in terms of classical paths. For a detailed analysis we now consider the power spectrum of $r_{11}$ with respect to length. This quantity, which is shown in Figure 3a, is given by the squared modulus of the Fourier transform of $r_{11}$ and will be denoted as $\mathcal{R}_{11}(L)$ in the following.

In complete agreement with reference [15], we can establish a correspondence between peaks of $\mathcal{R}_{11}$ and the classical trajectories including their repetitions. The first peak is not a classical trajectory contributing to reflection, but corresponds to diffraction off the lead mouths [13,15]. This effect can be interpreted in terms of a trajectory that gets reflected back at the right lead. For larger lengths $L$, we can identify a triangular path, a five-star path, a seven-star path, and so on. In agreement with the semiclassical quantization of the initial and final angle, the star-shaped paths are the most important ones for small mode numbers which favor the forward direction.

The resolution of the length spectrum is limited by the width of the momentum interval used for the Fourier transformation. While this can easily be controlled, there are also intrinsic effects restricting the resolution. Within a semiclassical picture, at given energy and mode numbers the angle quantization selects the appropriate paths. Depending on the width of the leads, the transverse position of the starting and end points in the leads are variable and therefore a given type of trajectories exists in a certain momentum interval. In the Fourier transformation these trajectories will contribute with different weights since the corresponding action will depend on the momentum, thus yielding a finite resolution. Already the fact that a type of trajectory effectively contributes only in a finite momentum interval may limit the resolution more strongly than the finite interval imposed by the numerics. In this respect it is also important to note that quantum mechanical diffraction effects at the lead mouths [13,15] influence the effective momentum interval and may be relevant for the resolution.

Placing a sufficiently high barrier into the cavity yields a reflection coefficient (not shown here) uncorrelated to that presented in Figure 2. On the other hand, we expect that individual trajectories would be greatly altered by the barrier and thus we analyze the length spectrum $\mathcal{R}_{11}(L, V_b)$ as a function of the barrier height. For very high barriers one can see in Figure 3b that new length scales have appeared rendering the identification more involved as compared to the case of vanishing barrier.

Some features are easily explained like the appearance of a peak at length $2R$, while in the absence of a barrier the minimum length is $4R$. In the presence of a high barrier, the direct path may get reflected at the barrier thus leading to a peak at half of the previous minimal length. The peak at $4R$ now consists of two contributions, namely the direct path which is reflected at the right lead and twice the direct path reflected at the barrier which involves a reflection at the left lead mouth. The hierarchy continues with a smaller peak at about $6R$ which stems from three repetitions of the direct path reflected at the barrier.

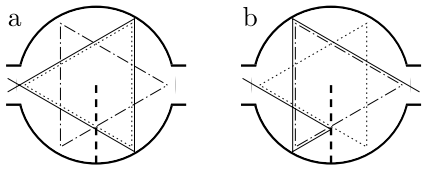


**Fig. 4.** The triangular path in the circular tunneling billiard may follow the dotted triangle or its mirror image shown as dashed-dotted line. a) Trajectory (solid line) which is transmitted at the barrier and contributes to the reflected trajectories in the billiard. b) Trajectory (solid line) which is reflected at the barrier and therefore contributes to the transmission through the billiard.

In principle, it is not clear that an analysis in terms of classical paths is applicable for arbitrary barrier height since tunneling necessarily implies non-classical trajectories. However, we will show that such an analysis is still possible and helpful towards the understanding of the transport problem. For instance, comparison between Figures 3a and b shows a large suppression of the harmonic coming from the triangular path, while the five-star path component is much less affected. Simple arguments given in the next section explain this difference in behaviour.

## 3 Paths in the presence of a tunnel barrier

For a semiclassical analysis of the energy-dependent transmission and reflection spectra, we first have to discuss how the classical paths are modified by the barrier. The cases where well-defined classical paths exist, are those of the circular billiard ($V_b = 0$) and the circular billiard with a very high barrier ($V_b = \infty$). While postponing a more detailed analysis to Section 4, we expect that at intermediate barrier heights, the transmission and reflection amplitudes for the billiard should be given by both classes of trajectories properly weighted according to the transmission and reflection coefficients of the barrier. The length spectrum of the reflection amplitude, referred to as reflection spectrum in the following, of the circular billiard shown in Figure 3a displays distinct peaks which can be associated with a triangle, a five-, and a seven-star. In the following discussion we will focus on these three trajectories.

We start with the triangular path as the simplest case. In the absence of a barrier, the trajectory just follows the triangle as shown in Figure 4a. As the barrier height $V_b$ is increased the transmission probability through the barrier decreases and for high barriers the original triangle is no longer a possible path. Accordingly, the peak in the reflection spectrum corresponding to the triangle will decrease in amplitude with increasing barrier height. For sufficiently large $V_b$, the possibility of reflection at the barrier has to be taken into account. As a consequence of this reflection the path will no longer continue on the original triangle shown as dotted line in Figure 4 but follow, at least for sufficiently thin barriers, the dashed-dotted line obtained as mirror image with respect to a vertical line through the barrier. It is important that this path has

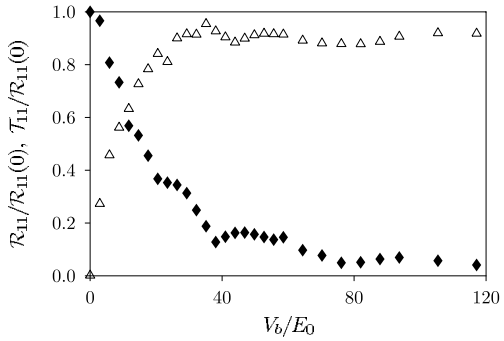


**Fig. 5.** Variation of the peak height in the length spectrum for the triangular path as a function of the barrier height $V_b$. The diamonds and triangles correspond to $\mathcal{R}_{11}$ and $\mathcal{T}_{11}$, respectively. Both quantities are normalized with respect to $\mathcal{R}_{11}(0)$, *i.e.* the case of vanishing barrier.

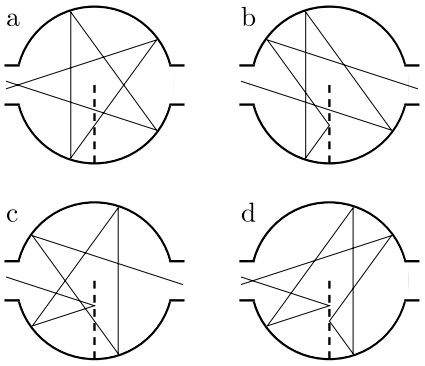


**Fig. 6.** Four different classes of paths related to the five-star: paths with two transmissions or two reflections at the barrier (a and d) contribute to the reflected trajectories in the billiard while paths with one transmission and one reflection at the barrier (b and c) contribute to the transmission through the billiard.

the same length as the original path. However, now the end point no longer lies in the entrance lead but in the opposite lead and thus the path reflected at the barrier will contribute to the transmission through the billiard. Correspondingly, the triangle will become more important in the transmission spectrum as the barrier height is increased. This qualitative discussion is confirmed by the numerical results for the reflection and transmission spectra, $\mathcal{R}_{11}$ and $\mathcal{T}_{11}$, shown in Figure 5 as diamonds and triangles, respectively.

While the triangular path cannot appear in the reflection spectrum for very high barriers, it is interesting to note that there is a peak at a length corresponding to two repetitions of the triangular path. This can readily be verified by comparing Figures 3a and b. While one reflection at the barrier changes the exit lead from the left to the right, an additional reflection restores the left lead as exit lead. Therefore, the peak can be identified with two repetitions of the path shown in Figure 4b including a reflection at the right lead due to diffraction at the lead mouth.

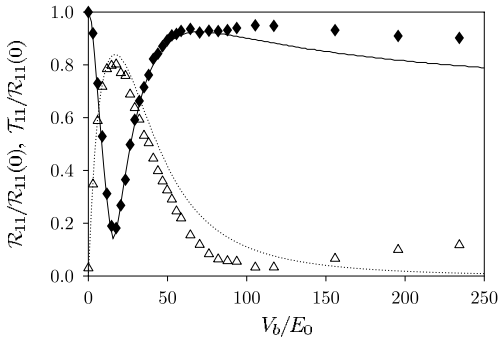


**Fig. 7.** Variation of the peak height in the length spectrum for the five-star trajectory as a function of the barrier height $V_b$. The diamonds and triangles correspond to $\mathcal{R}_{11}$ and $\mathcal{T}_{11}$, respectively. Both quantities are normalized with respect to $\mathcal{R}_{11}(0)$, *i.e.* the case of vanishing barrier. The solid and the dotted line give the results of a semiclassical calculation taking into account tunneling through the barrier.

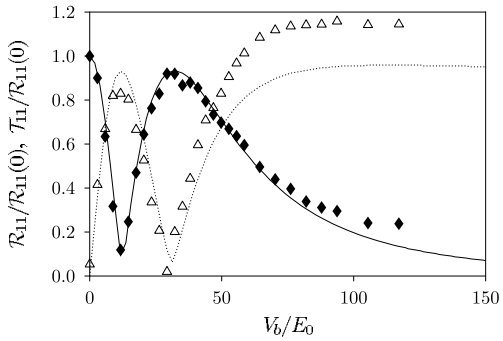


**Fig. 8.** Same as in Figure 7, but for the seven-star trajectory.

The behaviour of the five-star trajectory is more complex due to the fact that it crosses the barrier twice. Making use of the same geometrical arguments as for the triangle, we may distinguish four different classes of trajectories shown in Figure 6 which correspond to two transmissions at the barrier (a), one reflection and one transmission (b and c), and two reflections (d). In fact, since the trajectory may either start into the upper or lower half of the billiard, these four classes correspond to eight different trajectories which can be obtained by reading the diagrams in the forward and backward direction.

Like for the case of the triangle, a reflection at the barrier changes the sense of rotation in the circle thereby changing the exit lead. As can be seen from Figure 6, the paths with an even number of reflections (a and d) contribute to the reflected paths through the billiard while the paths with an odd number of reflections (b and c) contribute to the transmission through the billiard.

Let us first consider the trajectories contributing to the reflection. The trajectory (a) will only contribute for small barrier heights because it has to be transmitted through the barrier twice. On the other hand, the trajectory (d) will appear only for rather high barriers since it requires two reflections at the barrier. As a consequence, we expect that the peak in the reflection spectrum corresponding to the five-star trajectory will exhibit a minimum at intermediate barrier heights where none of the trajectories (a) and (d) contribute significantly. The other trajectories (b and c) appear in the transmission spectrum at intermediate barrier heights because they have to be reflected as well as transmitted once at the barrier.

We conclude from the discussion of the five-star trajectory that in general the dependence on barrier height of the peak heights in the transmission and reflection spectra should be nonmonotonic. This is confirmed by the numerical data shown as diamonds ($\mathcal{R}_{11}$) and triangles ($\mathcal{T}_{11}$) in Figure 7. The lines shown there are results of a semiclassical analysis which will be discussed in detail in the next section.

For this nonmonotonic behaviour it is crucial that the reflection of a classical path at the barrier does not change the length of the trajectory. Only then a change in the barrier height will not affect the position of the peak and contributions of different paths have to be coherently superposed.

The behaviour of the peak heights becomes more complex as the trajectories encounter the barrier more often. This will become clear from our final example, the seven-star trajectory. In this case, the trajectory encounters the barrier three times giving rise to eight classes of trajectories. We may classify these trajectories according to their behaviour at the barrier by assigning a T or an R for each transmission or reflection, respectively. Then, the paths contributing to the reflection spectrum are those containing an even number of R, namely TTT, RRT, RTR, and TRR. While the first trajectory will contribute for very small barriers, the other trajectories appear only for sufficiently high barriers. At very high barriers none of these paths is allowed. Accordingly, the peak in the reflection spectrum associated with the seven-star will initially decrease with increasing barrier height, exhibit a minimum followed by a maximum and then go to zero as the barrier height becomes very large. This behaviour can readily be verified by comparison with the numerical results for $\mathcal{R}_{11}$ shown as diamonds in Figure 8.

The behaviour of the transmission spectrum $\mathcal{T}_{11}$ shown in this figure as triangles can be understood along the same line of reasoning. The trajectories contributing to this spectrum are those with an odd number of reflections at the barrier, *i.e.* RTT, TRT, TTR, and RRR. Since there is at least one reflection at the barrier, seven-star trajectories may contribute to the transmission spectrum only for finite barrier heights. With increasing height there will be a maximum followed by a minimum and at very high barriers the RRR-trajectory will contribute.

So far, we have concentrated on trajectories which in the absence of a barrier contribute to the reflection. The behaviour of classical paths connecting two different leads, *i.e.* paths contributing to the transmission, as a function of the barrier height is slightly more complex. In this case, one has to distinguish the paths first going into the upper and lower half of the billiard. As an example, we consider the paths shown in Figure 9 which represent one half of an eight-star. From this figure it becomes clear that

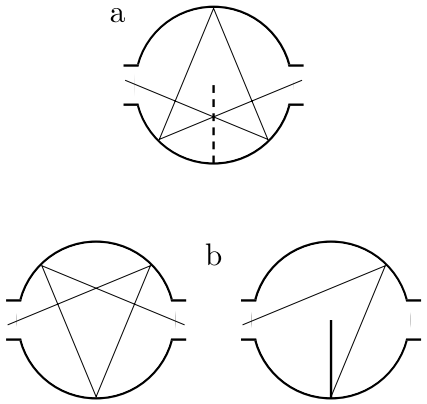


**Fig. 9.** Trajectory corresponding to a half of an eight-star trajectory. a) The trajectory starting into the lower half of the billiard contributes to the transmission through the billiard for arbitrary barrier height. b) The trajectory starting into the upper half of the billiard contributes to the transmission in the absence of a barrier (left) and to the reflection for high barrier (right).

depending on the incident angle of the path there will be an even or odd number of contacts with the barrier. Accordingly, the path shown in Figure 9a will behave very much like the five-star which also encounters the barrier twice. On the other hand, the path shown in Figure 9b has just one contact with the barrier and its dependence on the barrier height resembles that of the triangle. As a consequence, while both trajectories will contribute to the transmission for low barriers, only one of them (Fig. 9a) will do so at high barriers. The other path will turn into a reflected path (right part of Fig. 9b) instead.

This line of reasoning generally applies to trajectories which are transmitted in the absence of a barrier. Even though the analysis now becomes more complicated, these paths also lead to nonmonotonic reflection and transmission spectra as a function of barrier height. Again an increasing number of contacts with the barrier will lead to an increasing number of extrema. An example will be shown in Section 5 where the spectra of the total transmission are discussed (Fig. 13).

The previous qualitative discussion allowed us to understand the effect of a tunnel barrier by simple consideration of classical trajectories. In the next section we will show that a quantitative agreement with the exact calculations can be obtained within a semiclassical approach where the possibility of transmission or reflection at the barrier is incorporated.

## 4 Semiclassical description of the circular tunneling billiard

We now want to include tunneling into the semiclassical picture while remaining rather close to the expression for the semiclassical Green function (8) in terms of classical paths. To this end, we multiply the contribution of the classical paths by amplitudes $\alpha_t$ or $\alpha_r$ accounting for each transmission or reflection of the classical path at the barrier.

The treatment of a barrier of finite length in the circular tunneling billiard represents a rather complicated two-dimensional problem. However, we may approximately describe the behaviour of an electron at the barrier as a plane wave encountering a barrier of infinite length. Then the problem may be separated into the directions perpendicular and parallel to the barrier and the only parameter describing the scattering geometry is the incident angle $\phi$. At this point it is important to note that the sequence of transmissions and reflections at the barrier matters. For example the five-star trajectories shown in Figures 6b and c which, if read from left to right, correspond to TR and RT, respectively, have different incident angles for the transmission and reflection events.

For an infinitely long barrier the relevant momentum component is the one perpendicular to the barrier

$$k_\perp = k\cos(\phi). \tag{10}$$

We now may use the standard results for one-dimensional barrier penetration to approximate the transmission and reflection amplitudes by

$$\alpha_t(\phi) = \frac{2k_\perp k'_\perp \exp(-\mathrm{i}k_\perp b)}{2k_\perp k'_\perp \cos(k'_\perp b) - \mathrm{i}(k_\perp^2 + k_\perp'^2)\sin(k'_\perp b)} \tag{11}$$

$$\alpha_r(\phi) = \mathrm{i}\frac{k_\perp'^2 - k_\perp^2}{2k_\perp k'_\perp}\sin(k'_\perp b)\alpha_t, \tag{12}$$

respectively, where

$$k'_\perp = \left(k_\perp^2 - \frac{2MV_b}{\hbar^2}\right)^{1/2} \tag{13}$$

and $b$ is the width of the barrier. Expressions (11, 12) reduce to the usual one-dimensional expressions for incident angle $\phi = 0$.

We emphasize that it would not be sufficient to take the modulus of $\alpha_t$ and $\alpha_r$ since in general the contributions of different paths have to be added up coherently. In fact, destructive interference of paths is quite important for the interpretation of the barrier height dependence of the length spectra. As can be seen from (12), the relative phase factor between the reflected and the transmitted path is always $\pm\mathrm{i}$. Since changing a reflection at the barrier into a transmission and *vice versa* will change the exit lead, two classical paths going to the same exit lead differ by their behaviour at an even number of barrier encounters. Therefore, the relative phase factor will be $\pm 1$. In addition, a reflection at the barrier does not change the classical amplitude $\tilde{D}$, so that the two paths either interfere perfectly constructive or destructive.

As an example we consider the minimum in the peak height of the reflection spectrum corresponding to the five-star shown in Figure 7. There is such a pronounced minimum only because the two contributing paths, TT and RR (*cf.* Figs. 6a and d), interfere destructively. On the other hand, $\mathcal{R}_{11}$ is not vanishing at the minimum. This is due to the fact that the Fourier transformation has to

be taken over a finite energy interval. Since the barrier height at which the minimum occurs is energy-dependent, the minimum of $\mathcal{R}_{11}$ will be smeared out.

For finite barrier width, the phase factors appearing in the transmission and reflection amplitudes have an additional effect. The contribution of the barrier region to the total action of the path will depend on the barrier height which will result in an effective change of the length of the trajectory. This becomes more important as the width and height of the barrier are increased. However, for the parameters used here, the barrier is thin enough so that the change in length is below the resolution of the discrete Fourier transformation. Nevertheless, the peak height is affected. This may become important for sufficiently high barriers and cause the decrease in the reflection spectrum of the five-star (Fig. 7) at large $V_b$. For high barriers of finite width slight changes in the scattering geometry with respect to the ideal geometry for a thin barrier may also affect the peak height.

We now turn to a more detailed discussion of the quantum mechanical results and those obtained from the semiclassical approach just introduced. The data are compared in Figure 7 for the five-star trajectory and in Figure 8 for the seven-star. In both cases the diamonds and triangles correspond to the quantum mechanical results for $\mathcal{R}_{11}$ and $\mathcal{T}_{11}$, respectively, while the solid and dotted lines are the corresponding semiclassical results with the modifications described above.

The expressions for the reflection and transmission amplitudes (11) and (12) depend on the momentum component $k_\perp$ perpendicular to the barrier and the height $V_b$ and width $b$ of the barrier. The geometry of the classical path together with the Fermi energy determines $k_\perp$. In the quantum calculations the barrier was implemented by increasing on three lattice points the potential to $V_b$. For the curves shown in Figures 7 and 8 we used an effective barrier width of 3.5 lattice spacings.

From Figures 7 and 8 we find, that at not too high barriers the agreement between the quantum mechanical data and the semiclassical theory modified for tunneling is very good. On the other hand, for high barriers deviations do occur. This seems to be at odds with the fact that in the limit of infinite barrier the modified theory becomes equivalent to the usual semiclassical expansion.

A qualitative deviation appears for rather high barriers in the transmission spectrum of the five-star and the reflection spectrum of the seven-star where the quantum mechanical data saturate at a finite value. This has been checked for barriers as high as $703E_0$. On the other hand, the semiclassical result decreases to zero since at least one barrier transmission is needed in order to get a path which describes transmission through the billiard and has the length of a five-star. The same holds for paths which describe reflection at the billiard and have the same length as a seven-star.

This discrepancy may be explained by paths with length close to those of the five- or seven-star. As an example we consider the five-star for which the reflection spectrum in the absence of a barrier and the transmission

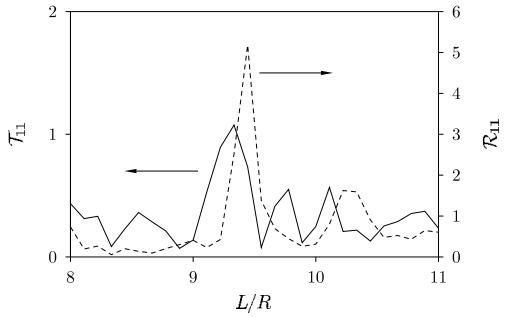


**Fig. 10.** Length spectra in the vicinity of the five-star peak. The dashed line corresponds to $\mathcal{R}_{11}$ in the absence of a barrier while the full line corresponds to $\mathcal{T}_{11}$ for a high barrier. The scales for $\mathcal{T}_{11}$ and $\mathcal{R}_{11}$ differ by a factor of three.

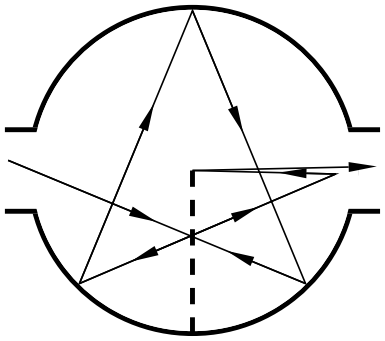

**Fig. 11.** Trajectory appearing in the transmission spectrum for high barriers at a length close to that of the five-star trajectory.

spectrum for very high barrier are shown in Figure 10 as dashed and solid lines, respectively. The highest peak of the dashed line indicates the length of the five-star. As expected, there is no peak at this position in the transmission spectrum. However, there exists a peak at somewhat smaller length which is broad enough to yield a contribution at the length of the five-star. The corresponding classical trajectory is shown in Figure 11. It involves three reflections at the barrier as well as a reflection at the exit lead, a quantum mechanical effect [15] already mentioned above.

These arguments also provide a partial explanation of the quantitative deviations found for high barriers in the reflection spectrum of the five-star trajectory and the transmission spectrum of the seven-star. In addition, as discussed in the previous section the discreteness of the Fourier transformation in combination with the change in path length as a function of barrier height results in another source of discrepancy.

While the agreement between the quantum mechanical and the semiclassical calculation demonstrates that for prominent peaks like the ones corresponding to the five- and seven-star the interpretation in terms of classical paths is possible, the deviations just discussed show that nevertheless the identification is not necessarily straightforward and requires a certain amount of caution. The dependence of peaks in the length spectrum on the barrier height may be of help in the identification since the

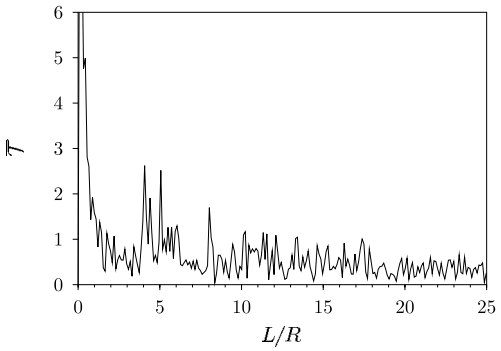


**Fig. 12.** Length spectrum of the total transmission $T$ for a circular billiard without barrier.

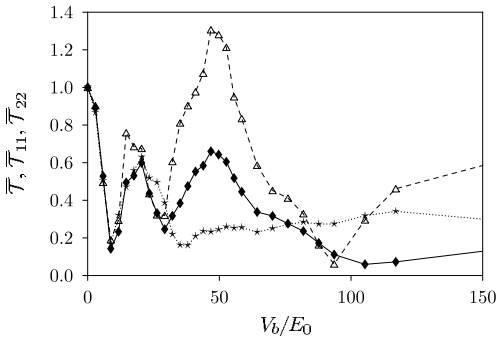


**Fig. 13.** Variation in the peak height of the transmission spectra $\overline{T}$ (diamonds), $\overline{T}_{11}$ (triangles), and $\overline{T}_{22}$ (stars) at $L = 4.1R$ as a function of the barrier height $V_b$. The data is normalized to the respective values at $V_b = 0$. The joining lines are guides to the eye.

number of extrema is related to the number of barrier encounters of the corresponding classical trajectory.

## 5 Total transmission and reflection in the circular tunneling billiard

The scattering amplitudes discussed above should be accessible to microwave experiments where the "Fermi energy" can be varied by changing the input frequency. A barrier could be introduced by placing a dielectric with a fine slit into the cavity. On the other hand, in transport experiments on ballistic microstructures it is the conductance which is measured. According to the Landauer formula, equation (2), the conductance through a cavity is proportional to the total transmission coefficient. Recently, measurements of transport through billiards with variable Fermi energy have been performed [7,22] so that it appears feasible to experimentally determine the length spectrum of the total transmission for the circular tunneling billiard. Since the semiclassical approaches developed so far provide a basis for the understanding of quantum transport, we would like to analyze now the effect of a barrier on the scattering probabilities.

The analysis for the transmission and reflection probabilities is more difficult than for the amplitudes because taking the squared modulus makes $|t_{nm}|^2$ depend on pairs of trajectories. Accordingly, a Fourier transformation yields peaks at lengths which correspond to differences between the lengths of two classical paths. Additionally, in order to calculate the total reflection or transmission, one has to take into account all scattering amplitudes $r_{nm}$ or $t_{nm}$ where the mode number is restricted by the Fermi energy *via* the maximum mode number $N$ introduced in Section 1. This will increase the number of different paths to be considered since at higher mode numbers paths enclosing a larger angle with the lead axis become relevant.

Moreover, when a new mode opens up it starts by being completely reflected, and the reflection coefficient jumps by one. This staircase effect will introduce high harmonics in the reflection coefficient which are not related to classical trajectories. Therefore we will focus our attention on the total transmission coefficient $T$.

As an example, the length spectrum of $T$ for the circular billiard without barrier is shown in Figure 12. Due to the large amount of possible length differences the spectrum is quite complex. Most of the peaks correspond not only to one pair of trajectories but to a combination of several pairs of approximately the same length difference. For example the highest peak, which is found at $L = 4.1R$, contains contributions of four different trajectories, namely a half of an eight-star (*cf.* Fig. 9), of a twelve-star, a sixteen-star, and a twenty-star. From these trajectories, three length differences, $4.20R$, $4.10R$, and $4.06R$, can be constructed which are all quite close to $L = 4.1R$. In principle, higher-order stars lead to further length differences in the same range. However, their contributions are negligible. Since the resolution of our discrete Fourier transformation is $0.1R$ and the typical peak width is twice as large (*cf.* Fig. 3), the contributions from the different combinations of trajectories cannot be resolved.

Given the complexity of the length spectrum, we may ask the question of whether the inclusion of a barrier can be treated as a perturbation that simply randomizes the phases of the contributing trajectories as do shape distortions [9,23,24] or magnetic field changes [4,12]. Our analysis in the previous sections suggests that this is not the case. The inclusion of a barrier has the effect of suppressing the contribution from certain trajectories while increasing that of the symmetry related ones, resulting in the nonmonotonic behaviour of the peaks in the length spectrum as a function of the barrier height which *cannot be interpreted as conductance fluctuations.*

In Figure 13 we present the dependence of the length spectrum on the barrier height for the total transmission coefficient as well as two individual probabilities, $|t_{11}|^2$ and $|t_{22}|^2$. In the following, these spectra are referred to as $\overline{T}$, $\overline{T}_{11}$, and $\overline{T}_{22}$, respectively. The data is given for the peak at $L = 4.1R$ to which several paths contribute as discussed above.

The nonmonotonic behaviour resulting from the dependence of the individual trajectories (of the contributing pairs) on $V_b$ illustrates the interplay between semiclassics and tunneling. The fact that $\overline{T}$ as well as $\overline{T}_{11}$ and $\overline{T}_{22}$

roughly exhibit the same structure implies that the same pairs of paths contribute to various transmission probabilities provided the momentum interval is large enough. Of course, predicting the peak height dependence as we did for the scattering amplitudes is more difficult since the relative weight and the phases of the trajectories of the contributing pairs become relevant. We therefore do not attempt to attain the agreement of Section 4.

Instead, we will give a qualitative explanation for the difference between $\overline{\mathcal{T}}_{11}$ and $\overline{\mathcal{T}}_{22}$. With growing number of reflections at the circle, the incident angle of the half-star trajectories decreases, thus suppressing the contribution of the higher-order stars, especially to $\overline{\mathcal{T}}_{22}$. Since the higher-order stars lead to more extrema in the $V_b$ dependence, the number of extrema of $\overline{\mathcal{T}}_{22}$ should be smaller than that of $\overline{\mathcal{T}}_{11}$. This is consistent with the numerical results of Figure 13. The number of extrema suggests that the dominant contribution to $\overline{\mathcal{T}}_{22}$ stems from the combination of one half of an eight- and of a twelve-star. One half of a sixteen-star should yield a contribution with a second minima for which there is no clear indication. On the other hand, $\overline{\mathcal{T}}_{11}$ displays a second broad maximum which is probably a combination of all the extrema from higher stars.

Obviously, the experimental resolution is limited and it would not be possible to observe a length spectrum as structured as that of Figure 12. In mesoscopic systems temperature plays two roles. On one hand, it controls the inelastic processes like electron-electron and electron-phonon interactions. This results in a cut-off length beyond which no trajectory should contribute in the coherent semiclassical expansion (8). The other effect of temperature is the rounding of the Fermi surface that, within our semiclassical approach, cuts the large length differences. Absorption processes in microwave cavities provide a cut-off length for the description in terms of classical trajectories, but in state-of-the-art experiments [3] this characteristic length can be much larger than the system size.

## 6 Conclusions

In this work we have studied quantum mechanically and semiclassically the effect of a tunneling barrier on quantum transport through ballistic cavities. This effect is most evident in the length spectra, *i.e.* the Fourier transform of the energy-dependent transmission and reflection amplitudes of the cavity. We have shown that the peak heights in the quantum mechanical length spectrum exhibit a nonmonotonic variation upon increasing the barrier height. This behaviour is quantitatively reproduced by combining a semiclassical approach to conductance with a simple model for barrier reflection and transmission of paths. The model provides furthermore an intuitive physical picture of the underlying process leading to the variations in the peak heights: they reflect the superposition of coherent contributions from paths being reflected at or transmitted through the barrier.

This mechanism is a clear-cut manifestation of tunneling orbits in the conductance of quantum billiards, which should be in principle observable in experiments. The effect of the tunnel barrier on individual peaks in the *length* spectrum manifests itself in the energy-dependent transmission and reflection coefficients.

We have also performed a corresponding analysis of the effect of a tunnel barrier on the *area* spectrum, the Fourier transform of the magnetic field dependent transmission at fixed Fermi energy. However, in that case a semiclassical analysis of the quantum mechanical results is more involved for two reasons: Firstly, the areas of the trajectories are no longer unchanged by a reflection at the barrier. Increasing the barrier height leads to a shift of the spectrum to small areas [9,17]. Secondly, in order to obtain well-resolved peaks in the area spectrum one has to perform the Fourier transformation over a rather large range of magnetic fields. Then, the condition that the cyclotron radius is much larger than the system size is no longer fulfilled in our numerical calculations and the shapes of the trajectories become field-dependent. This leads to broadening and thus to a severe restriction of resolution. For high magnetic fields one may even find splitting of the peaks in the area spectrum. Hence in most cases it will be hard to unambiguously identify peaks in the area spectrum.

Low-frequency structure has been obtained in the (non-averaged) experimental area spectra of ballistic microstructures [4,9]. The observed peaks correspond to areas close to those of the shortest periodic orbits. However, a clear identification between peaks and trajectories has not been possible to establish. As discussed above the analysis becomes quite difficult when pairs instead of single trajectories are involved. Thus, a certain amount of caution has to be exerted for a detailed interpretation in terms of classical trajectories.

We have shown that the length spectrum admits a simple semiclassical analysis, *even in the presence of tunneling*. In view of microwave experiments [3] as well as recent work on cavities in two-dimensional electron gases [22] which has demonstrated the possibility of measuring length spectra, it seems feasible to experimentally verify the nonmonotonic dependence on the barrier height discussed here.

We thank T. Fischaleck for useful discussions. Partial financial support was provided by DAAD and A.P.A.P.E. through the Procope program.

## References

1. C.W.J. Beenakker, H. van Houten, in *Solid State Physics*, Vol. 44, edited by H. Ehrenreich, D. Turnbull (Academic Press, San Diego, 1991).
2. S. Datta, *Electronic Transport in Mesoscopic Systems* (Cambridge University Press, Cambridge, 1995); Y. Imry, *Introduction to Mesoscopic Physics* (Oxford University

Press, New York, 1997); T. Dittrich, P. Hänggi, G.-L. Ingold, B. Kramer, G. Schön, W. Zwerger, *Quantum Transport and Dissipation* (Wiley-VCH, Weinheim, 1998).
3. H.-J. Stöckmann, J. Stein, Phys. Rev. Lett. **64**, 2215 (1990); H.-D. Gräf, H.L. Harney, H. Lengeler, C.H. Lewenkopf, C. Rangacharyulu, A. Richter, P. Schardt, H.A. Weidenmüller, Phys. Rev. Lett. **69**, 1296 (1992); M. Kollmann, J. Stein, U. Stoffregen, H.-J. Stöckmann, B. Eckhardt, Phys. Rev. E **49**, R1 (1994).
4. C.M. Marcus, A.J. Rimberg, R.M. Westervelt, P.F. Hopkins, A.C. Gossard, Phys. Rev. Lett. **69**, 506 (1992); C.M. Marcus, R.M. Westervelt, P.F. Hopkins, A.C. Gossard, Chaos **3**, 643 (1993).
5. M.W. Keller, O. Millo, A. Mittal, D.E. Prober, R.N. Sacks, Surf. Sci. **305**, 501 (1994).
6. M.J. Berry, J.H. Baskey, R.M. Westervelt, A.C. Gossard, Phys. Rev. B **50**, 8857 (1994).
7. M.W. Keller, A. Mittal, J.W. Sleight, R.G. Wheeler, D.E. Prober, R.N. Sacks, H. Shtrikmann, Phys. Rev. B **53**, R1693 (1996).
8. A.M. Chang, H.U. Baranger, L.N. Pfeiffer, K.W. West, Phys. Rev. Lett. **73**, 2111 (1994).
9. Y. Lee, G. Faini, D. Mailly, Chaos, Solit. Fract. **8**, 1325 (1997); Y. Lee, G. Faini, D. Mailly, Phys. Rev. B **56**, 9805 (1997).
10. R.P. Taylor, R. Newbury, A.S. Sachrajda, Y. Feng, P.T. Coleridge, C. Dettmann, N. Zhu, H. Guo, A. Delage, P.J. Kelly, Z. Wasilewski, Phys. Rev. Lett. **78**, 1952 (1997).
11. M.C. Gutzwiller, *Chaos in Classical and Quantum Mechanics* (Springer, New York, 1990); M. Brack, R.K. Bhaduri, *Semiclassical Physics* (Addison-Wesley, Reading, 1997).
12. R.A. Jalabert, H.U. Baranger, A.D. Stone, Phys. Rev. Lett. **65**, 2442 (1990); H.U. Baranger, R.A. Jalabert, A.D. Stone, Chaos, **3**, 665 (1993).
13. H. Ishio, J. Burgdörfer, Phys. Rev. B **51**, 2013 (1995).
14. W.A. Lin, R.V. Jensen, Phys. Rev. B **53**, 3638 (1996).
15. C.D. Schwieters, J.A. Alford, J.B. Delos, Phys. Rev. B **54**, 10652 (1996).
16. R.E. Prange, E. Ott, T.M. Antonsen Jr., B. Georgeot, R. Blümel, Phys. Rev. E **53**, 207 (1996); R. Blümel, T.M. Antonsen Jr., B. Georgeot, E. Ott, R.E. Prange, Phys. Rev. E **53**, 3284 (1996); R. Blümel, T.M. Antonsen, B. Georgeot, E. Ott, R.E. Prange, Phys. Rev. Lett. **76**, 2476 (1996).
17. M.J. Berry, J.A. Katine, R.M. Westervelt, A.C. Gossard, Phys. Rev. B **50**, 17721 (1994).
18. D.S. Fisher, P.A. Lee, Phys. Rev. B **23**, 6851 (1981).
19. A.D. Stone, A. Szafer, IBM J. Res. Develop. **32**, 384 (1988).
20. P.A. Lee, D.S. Fisher, Phys. Rev. Lett. **47**, 882 (1981).
21. H.U. Baranger, D.P. DiVincenzo, R.A. Jalabert, A.D. Stone, Phys. Rev. B **44**, 10637 (1991).
22. I.V. Zozoulenko, R. Schuster, K.-F. Berggren, K. Ensslin, Phys. Rev. B **55**, R10209 (1997).
23. H. Bruus, A.D. Stone, Phys. Rev. B **50**, 18275 (1994).
24. I.H. Chan, R.M. Clarke, C.M. Marcus, K. Campman, A.C. Gossard, Phys. Rev. Lett. **74**, 3876 (1995).